Report

Current Biology

A Color Vision Circuit for Non-Image-Forming Vision in the Primate Retina

Graphical Abstract

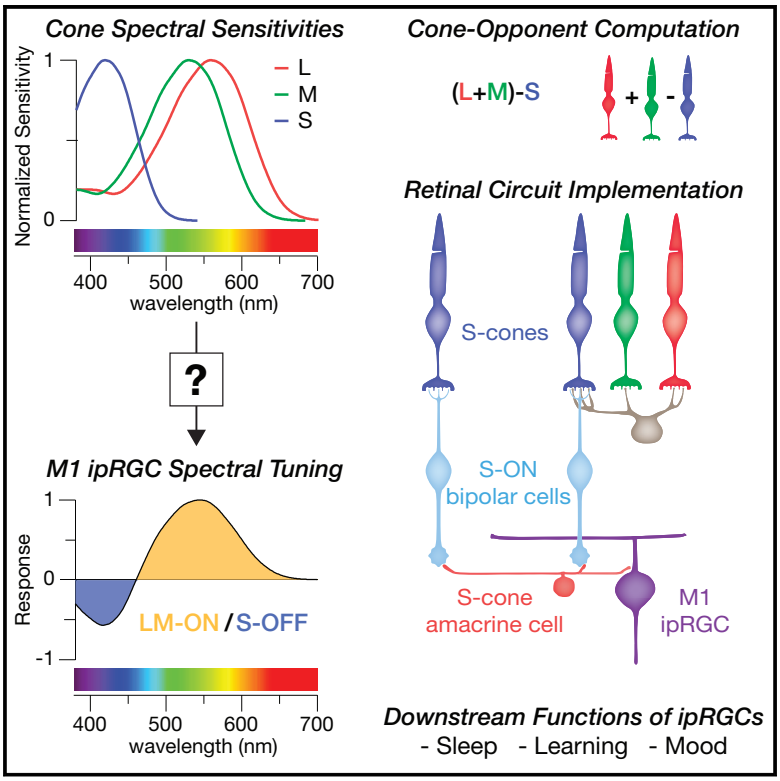

Highlights

- 3D reconstruction of the S-cone connectome revealed S-cone selective amacrine cells
- S-cone amacrine cells receive excitatory input from only S-cone ON bipolar cells
- S-cone amacrine cells make targeted inhibitory synapses onto ipRGCs
- Resulting short-wavelength sensitivity is distinct from that mediated by melanopsin

Authors

Sara S. Patterson, James A. Kuchenbecker, James R. Anderson, Maureen Neitz, Jay Neitz

Correspondence

jneitz@uw.edu

In Brief

Patterson et al. identify a new amacrine cell type in the primate retina with "blue" S-cone circuit input and targeted output to intrinsically photosensitive retinal ganglion cells (ipRGCs). This circuit may contribute to the effects of short-wavelength light on ipRGC downstream non-image-forming visual functions such as sleep, mood, and learning.

Patterson et al., 2020, Current Biology *30*, 1–6
April 6, 2020
https://doi.org/10.1016/j.cub.2020.01.040

CellPress

Please cite this article in press as: Patterson et al., A Color Vision Circuit for Non-Image-Forming Vision in the Primate Retina, Current Biology (2020), https://doi.org/10.1016/j.cub.2020.01.040

Current Biology
Report

A Color Vision Circuit for Non-Image-Forming Vision in the Primate Retina

Sara S. Patterson,[1,2] James A. Kuchenbecker,[2] James R. Anderson,[3] Maureen Neitz,[2] and Jay Neitz[2,4,*]
[1]Graduate Program in Neuroscience, University of Washington, Seattle, WA 98195, USA
[2]Department of Ophthalmology, University of Washington, Seattle WA 98109, USA
[3]Department of Ophthalmology and Visual Sciences, John A. Moran Eye Center, University of Utah School of Medicine, Salt Lake City, UT 84132, USA
[4]Lead Contact
*Correspondence: jneitz@uw.edu
https://doi.org/10.1016/j.cub.2020.01.040

SUMMARY

Melanopsin-expressing, intrinsically photosensitive retinal ganglion cells (ipRGCs) synchronize our biological clocks with the external light/dark cycle [1]. In addition to photoentrainment, they mediate the effects of light experience as a central modulator of mood, learning, and health [2]. This makes a complete account of the circuity responsible for ipRGCs' light responses essential to understanding their diverse roles in our well-being. Considerable progress has been made in understanding ipRGCs' melanopsin-mediated responses in rodents [3–5]. However, in primates, ipRGCs also have a rare blue-OFF response mediated by an unknown short-wavelength-sensitive (S)-cone circuit [6]. Identifying this S-cone circuit is particularly important because ipRGCs mediate many of the wide-ranging effects of short-wavelength light on human biology. These effects are often attributed to melanopsin, but there is evidence for an S-cone contribution as well [7, 8]. Here, we tested the hypothesis that the S-OFF response is mediated by the S-ON pathway through inhibitory input from an undiscovered S-cone amacrine cell. Using serial electron microscopy in the macaque retina, we reconstructed the neurons and synapses of the S-cone connectome, revealing a novel inhibitory interneuron, an amacrine cell, receiving excitatory glutamatergic input exclusively from S-ON bipolar cells. This S-cone amacrine cell makes highly selective inhibitory synapses onto ipRGCs, resulting in a blue-OFF response. Identification of the S-cone amacrine cell provides the missing component of an evolutionarily ancient circuit using spectral information for non-image forming visual functions.

RESULTS

3D Reconstruction of the Primate S-Cone Connectome

Primate ipRGCs have a rare yellow-ON, blue-OFF color tuning and respond to increased activity in L- and M-cone pathways and decreased activity in S-cone pathways (i.e., LM-ON/S-OFF cone opponency) [6]. The neural basis for the ipRGC's color tuning remains an open question. The S-OFF responses are blocked by L-AP4, an ON-pathway agonist, indicating an amacrine cell inhibition may invert the output of S-ON bipolar cells [9–12]. However, the mammalian retina contains 20–40 amacrine cell types, making selective identification of one undiscovered type difficult [13, 14]. Moreover, given the rarity of S-cones [15], little is known about the diversity of pathways carrying S-cone signals. To investigate the circuit mechanisms responsible for the ipRGC's S-OFF response, we used serial electron microscopy (EM) to reconstruct the neurons and synapses of the primate S-cone connectome from a volume of macaque inferior retina at ~1–1.5 mm eccentricity, near the peak density for ipRGCs [16]. The resulting dataset of nearly 2,000 sections spanned from the outer nuclear layer to the nerve fiber layer, enabling us to reconstruct complete circuits in 3D and identify the synaptic contacts between neurons.

Reliable identification of upstream S-cone circuitry is essential for identifying a novel S-cone neuron, and thus, we began by reconstructing the established S-cone connectome, building on our previous reconstructions of S-cone bipolar cells in the outer retina [17]. Briefly, S-cones were distinguished from L/M-cones by their highly stereotyped post-synaptic contacts [18]. Each S-cone provides input to one to three S-ON bipolar cells and a single OFF midget bipolar cell (Figure 1A). The S-ON bipolar cells are highly cone-type specific and contact multiple S-cones, often passing several L/M-cones without contact to reach neighboring S-cones [19]. Using these features, we confidently identified eight S-cones and 14 S-ON bipolar cells.

Here, we extended these S-ON pathway reconstructions to the inner retina. The terminals of each bipolar cell type stratify at a stereotyped location within the inner retina, providing excitatory glutamatergic input to amacrine and retinal ganglion cells (RGCs) stratifying in the same layer [20]. Each of the 14 S-ON bipolar cells stratified in the innermost layer of the inner retina, sublamina 5 (S5), closest to the ganglion cell layer (GCL) [19] (Figures 1A and 1B). We further verified S-ON bipolar cell identity by reconstructing their best-known output: small bistratified RGCs (Figures 1B and 1C) [21, 22]. Each S-ON bipolar cell contacted two or three small bistratified RGCs, and the most complete small bistratified RGCs collected inputs from up to nine S-ON bipolar cell terminals. The S-cone exclusive inner dendritic tier of each small bistratified RGC served as a bridge within the inner

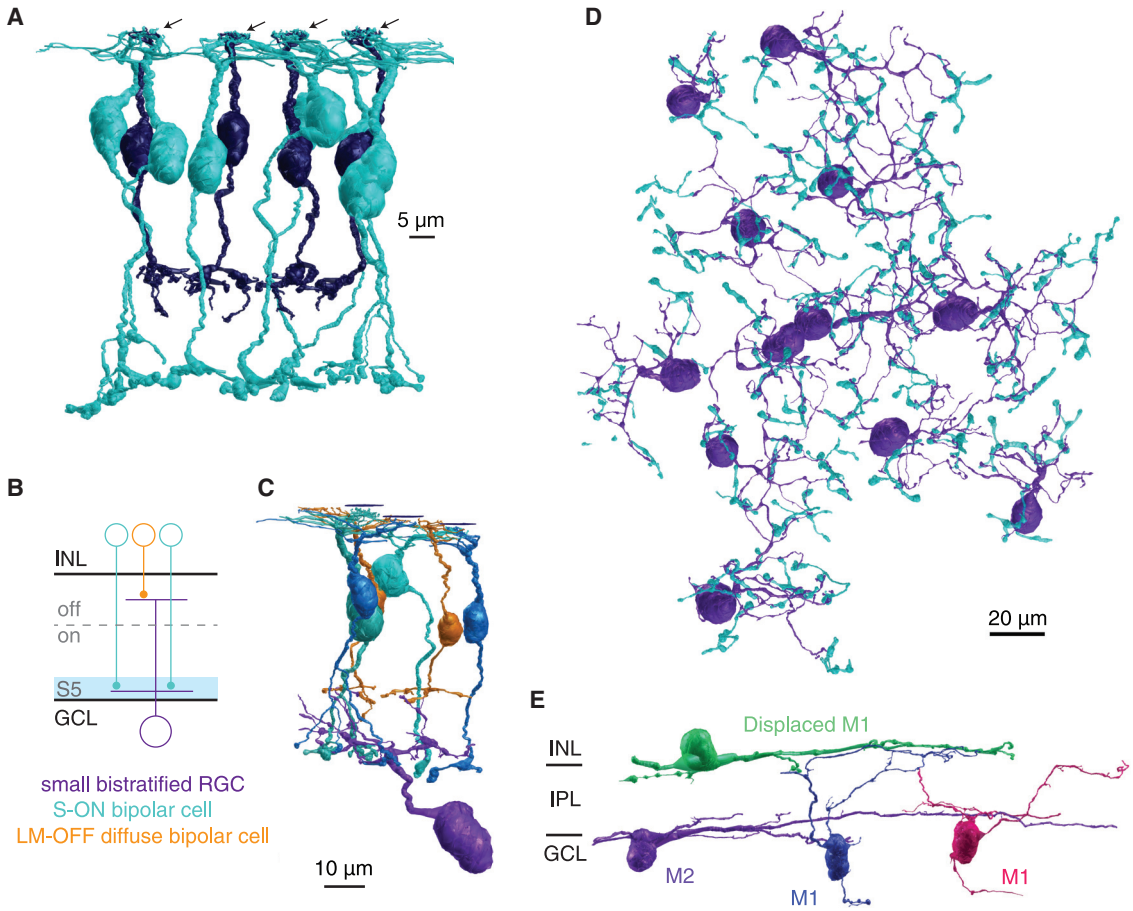

Figure 1. Serial EM Reconstruction of ipRGCs and the S-Cone Connectome in Primate Retina

(A) Four representative S-cones (arrows) and their S-ON bipolar cell (blue) and OFF midget bipolar cell (purple) contacts.

(B) Small bistratified RGC circuit used for verification of S-cone and S-ON bipolar cell identification.

(C) 3D reconstruction of the small bistratified RGC circuit in (B).

(D) 60 S-ON bipolar cell terminals contacting 12 small bistratified RGCs.

(E) 3D reconstructions of the major ipRGC subtypes in primate retina. Note the ipRGC dendrites are monostratified but appear curved because the volume slopes away from the fovea.

retina to identify an additional 46 S-ON bipolar cell terminals. In total, we reconstructed 60 S-ON bipolar cell terminals, each confirmed by extensive synaptic contacts with at least one of 12 small bistratified RGCs (Figure 1D).

A Novel S-Cone Selective Amacrine Cell Links S-ON Bipolar Cells to ipRGCs

We next reconstructed the two major ipRGC subtypes reported in the primate retina, which are distinguished by their stratification in the outermost and innermost edges of the inner retina and are thought to correspond to M1 and M2 ipRGCs, respectively [16, 23, 24] (Figure 1E). The dendrites of both ipRGCs branched sparsely, with dendritic fields extending beyond the edges of the volume. We focused our efforts on M1 ipRGCs with somas in the GCL and dendrites stratifying primarily in the outermost layer of the inner retina, sublamina 1 (S1). The M1 ipRGC's stratification in S1 limits the opportunities for contact with amacrine cells receiving S-ON bipolar cell input on the opposite side of the inner retina in S5.

Taken together, our reconstructions of the established S-cone circuitry and ipRGCs provided the necessary infrastructure to effectively search for the source of the S-OFF response. To identify candidate S-cone amacrine cells, we reconstructed neurons postsynaptic to the ribbon synapses in S-ON bipolar cell terminals (Figure 2A and 2B). Although many amacrine cells stratifying in S5 received occasional S-ON bipolar cell input, a population of medium-field displaced amacrine cells recognizable by their distinctive soma ultrastructure (Figure 2D) were ultimately identified as exclusively contacting S-ON bipolar cells (Figure 2C). In the inner retina, the amacrine cells' thin, sparse processes co-stratified narrowly with the S-ON bipolar cell terminals in S5. Their dendritic fields covered the S-ON bipolar cell terminal mosaic, each collecting input from over 10 S-ON bipolar cell terminals. Of the 102 bipolar cell inputs to the three most complete amacrine cells, all but six were from confirmed S-ON bipolar cells.

Amacrine cell processes are typically confined to the inner retina, however, some S-cone amacrine cells also extended processes into the GCL. Strikingly, these processes contacted an

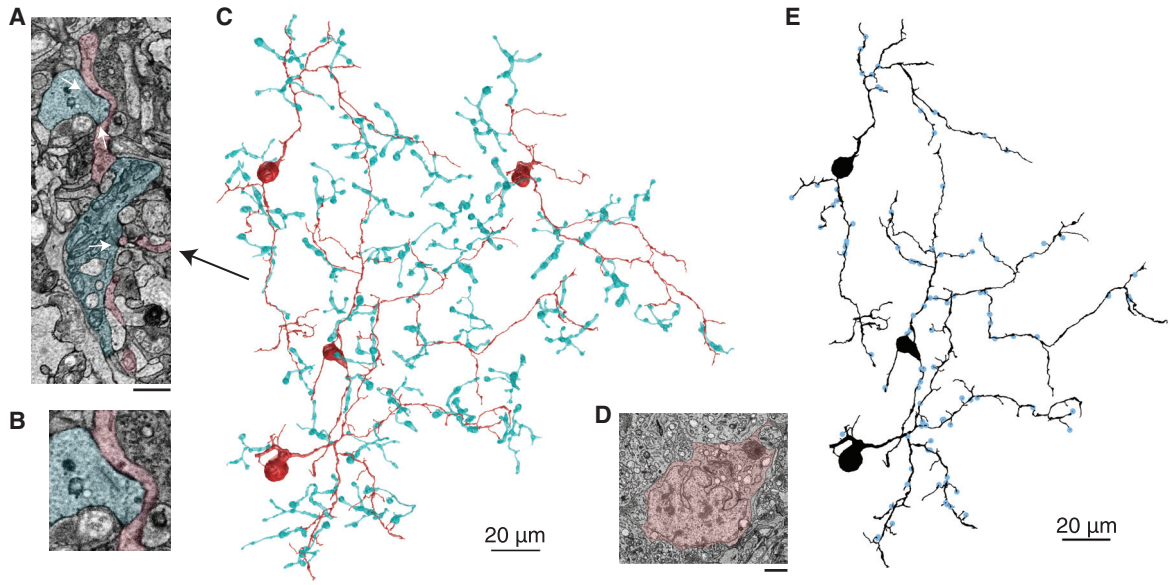

Figure 2. Identification of an S-Cone-Exclusive Amacrine Cell

(A) Electron micrographs of three ribbon synapses (white arrows) from an S-ON bipolar cell (cyan) to an S-cone amacrine cell (red). Scale bar: 1.5 µm.

(B) Inset from (A) showing two S-ON bipolar cell ribbon synapses.

(C) 3D reconstructions of S-ON bipolar cell axon terminals (cyan) providing input to four S-cone amacrine cells (red).

(D) S-cone amacrine cells are easily identifiable by their asymmetric nuclei offset from the center of their soma. Scale bar: 1 µm.

(E) Locations of S-ON bipolar cell input (blue) to three S-cone amacrine cells.

M1 ipRGC soma (Figure 3A; Video S1). Moreover, thin branches extended from the ipRGC's cell body to receive additional input from the S-cone amacrine cell processes. Small branches extending from the primary dendrites were also observed receiving input from S-cone amacrine cells within the inner retina (Figures 3F and 3G).

M1 ipRGCs Receive Targeted Synaptic Input from S-Cone Amacrine Cells

We next examined the synaptic connections between S-cone amacrine cells and ipRGCs, focusing on the three most complete S-cone amacrine cell reconstructions. Conventional synapses, which are traditionally assumed to be inhibitory, were identified as a cluster of vesicles on the pre-synaptic neuron adjacent to a membrane density on the post-synaptic neuron. Figures 3B–3E and 3H show S-cone amacrine cell synapses onto the ipRGC soma and branches within the inner retina and GCL. This unique concentration of S-cone-exclusive inhibition near the action potential initiation site could provide modulatory control over synaptic inputs received throughout the ipRGC's dendritic field [26]. The somas of human ipRGCs and other RGCs have been reported to receive GABAergic input [24, 27, 28], and the S-cone amacrine cell's morphology is consistent with a GABAergic amacrine cell [29]. Moreover, this motif is distinct from the previously identified glycinergic S-cone amacrine cell in ground squirrel that stratifies diffusely, collecting S-ON bipolar cell input in S5 and providing S-cone inhibition to non-ipRGC ganglion cells stratifying in S1 [10, 30]. Based on strong morphological similarities, stratification, and displaced soma, the primate S-cone amacrine cell is likely the homolog to the MA-S5 amacrine cell in mouse [31] and the A12 amacrine cell in human, cat, and ground squirrel [32].

To visualize the extent of S-cone convergence onto M1 ipRGCs, we plotted the network of upstream S-cone exclusive circuits (Figure 3I). Each S-ON bipolar cell collects input from an overlapping set of 2–3 S-cones, as in Figure 1A. The network in Figure 3I is likely an underestimate at both the level of S-ON bipolar input to S-cone amacrine cells and S-cone amacrine cell input to ipRGCs, because we only included ipRGCs with somas within our EM volume and occasional S-cone amacrine cell processes extended past the edges of the volume or could not be reliably annotated. Nevertheless, the high degree of S-cone convergence suggests S-cone amacrine cell input to M1 ipRGCs contributes a strong S-cone signal.

DISCUSSION

Short-wavelength cone-exclusive ON bipolar cells are a highly conserved feature of mammalian retinas [33, 34] forming the basis of the primordial color vision circuit comparing long- and short-wavelength light [35]. Here, we show that this circuit extends to the inner retina, with an additional S-cone exclusive neuron, an amacrine cell receiving only S-ON bipolar cell input. The concept of a primordial color vision circuit has been considered as the precursor to the primate hue perception circuitry, however, our findings suggest this ancient color vision circuit is instead still serving its original function. Much of the S-cone amacrine cell's output is targeted to ipRGCs, another highly conserved neuron mediating ancient non-image-forming visual functions. Accordingly, the S-cone amacrine cell may be part of an evolutionarily ancient color vision circuit, not for hue perception, but for non-image-forming vision.

The downstream functions of the M1 ipRGCs are among the best characterized of all RGCs [36]. Thus, our results establish

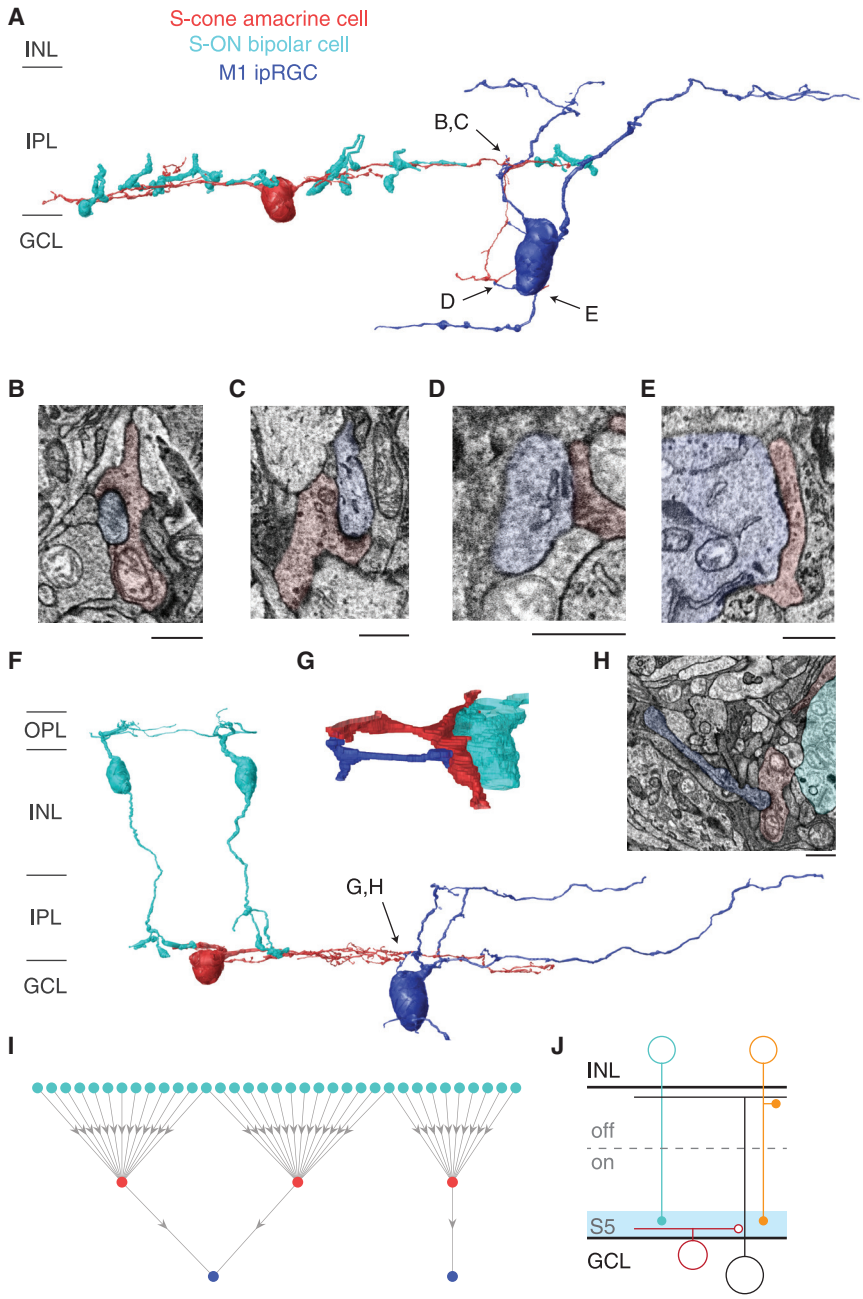

Figure 3. M1 ipRGCs Receive Targeted Inhibitory Input from S-Cone Amacrine Cells

(A) 3D reconstruction of an M1 ipRGC receiving synaptic input from an S-cone amacrine cell. The S-cone amacrine cell dendrite travels into the GCL to provide additional synaptic input to the M1 ipRGC soma. See also Video S1.

(B–E) Four electron micrographs of representative synapses between the S-cone amacrine cell and M1 ipRGC in (A). (B) and (C) show examples of synapses onto M1 ipRGC branches in the inner retina, (D) shows an M1 ipRGC process receiving synaptic input in the GCL, and (E) shows synaptic input to the M1 ipRGC soma.

(F) 3D reconstruction of S-cone amacrine cell input to an M1 ipRGC, with complete reconstructions of two representative S-ON bipolar cells.

(G) Detailed reconstruction of S-cone amacrine cell to ipRGC synaptic contact.

(H) Synapse from an S-cone amacrine cell to the M1 ipRGC in (F) and (H). Scale bar: 1 μm.

(I) Network of S-ON bipolar cells, S-cone amacrine cells, and M1 ipRGCs.

(J) Circuit diagram of cone-opponent inputs to ipRGCs. *En passant* synapses from ON diffuse bipolar cells (orange) contribute to the LM-ON response [16, 25].

the S-cone amacrine cell among the few amacrine cell types to be placed within the context of a specific retinal circuit with an established visual function. The high degree of cone specificity demonstrated in Figure 2C indicates a crucial role for the S-cone amacrine cell. For example, the evolutionary pressure to know the time of day is strong, and color-opponent circadian photoentrainment is well-established in many vertebrates [37, 38]. As the sun rises and sets, the spectral contrast of the sky changes dramatically, with peaks in L/M- versus S-cone contrast at sunrise and sunset [39–41]. The S-cones providing input to the S-cone amacrine cell receive feedback from L/M-cones, effectively encoding the S-cone contrast relative to L/M-cone contrast [42]. This cone-opponent signal is conveyed to inner retinal neurons by the S-ON bipolar cells [43]. Thus, the output of the S-cone amacrine cell is predicted to be color-opponent (S-ON/LM-OFF) and is well-suited to encode the reliable circadian changes in the color of the sky.

STAR★METHODS

Detailed methods are provided in the online version of this paper and include the following:

- KEY RESOURCES TABLE
- LEAD CONTACT AND MATERIALS AVAILABILITY
- EXPERIMENTAL MODEL AND SUBJECT DETAILS

SUPPLEMENTAL INFORMATION

Supplemental Information can be found online at https://doi.org/10.1016/j.cub.2020.01.040.

ACKNOWLEDGMENTS

We thank Fred Rieke for helpful discussions; Andrea Bordt, David Marshak, and Judy Ogilvie for sharing their serial EM expertise; and Ed Parker for excellent technical assistance. Tissue was provided by the Tissue Distribution Program at the Washington National Primate Research Center (WaNPRC) with the help of Chris English. This work was supported by NIH grants R01-EY027859 (J.N.), T32-NS099578 (S.S.P.), T32-EY007031 (S.S.P.), R01-EY028927 (J.R.A.), P30-EY001730, P30-EY014800, and Research to Prevent Blindness.

AUTHOR CONTRIBUTIONS

J.N., M.N., and S.S.P. conceived the project, designed experiments, and wrote the paper. J.A.K., J.N., and M.N. acquired the volume. J.R.A. and J.A.K. built the volume. J.R.A. created the annotation software. S.S.P. created the visualization software, performed the experiments, and analyzed the data.

DECLARATION OF INTERESTS

The University of Washington has submitted provisional patent application (628504893) disclosing Systems, Methods, and Devices for Stimulating Circadian Rhythms (Authors: S.S.P., J.A.K., M.N., J.N.).

Received: December 5, 2019
Revised: January 8, 2020
Accepted: January 13, 2020
Published: February 20, 2020

REFERENCES

1. Berson, D.M. (2003). Strange vision: ganglion cells as circadian photoreceptors. Trends Neurosci. *26*, 314–320.
2. LeGates, T.A., Fernandez, D.C., and Hattar, S. (2014). Light as a central modulator of circadian rhythms, sleep and affect. Nat. Rev. Neurosci. *15*, 443–454.
3. Milner, E.S., and Do, M.T.H. (2017). A Population Representation of Absolute Light Intensity in the Mammalian Retina. Cell *171*, 865–876.e16.
4. Berson, D.M., Dunn, F.A., and Takao, M. (2002). Phototransduction by retinal ganglion cells that set the circadian clock. Science *295*, 1070–1073.
5. Wong, K.Y. (2012). A retinal ganglion cell that can signal irradiance continuously for 10 hours. J. Neurosci. *32*, 11478–11485.
6. Dacey, D.M., Liao, H.-W., Peterson, B.B., Robinson, F.R., Smith, V.C., Pokorny, J., Yau, K.-W., and Gamlin, P.D. (2005). Melanopsin-expressing ganglion cells in primate retina signal colour and irradiance and project to the LGN. Nature *433*, 749–754.
7. Rea, M.S., Figueiro, M.G., Bullough, J.D., and Bierman, A. (2005). A model of phototransduction by the human circadian system. Brain Res. Brain Res. Rev. *50*, 213–228.
8. Gooley, J.J., Rajaratnam, S.M.W., Brainard, G.C., Kronauer, R.E., Czeisler, C.A., and Lockley, S.W. (2010). Spectral responses of the human circadian system depend on the irradiance and duration of exposure to light. Sci. Transl. Med. *2*, 31ra33.
9. Neitz, J., and Neitz, M. (2011). The genetics of normal and defective color vision. Vision Res. *51*, 633–651.
10. Chen, S., and Li, W. (2012). A color-coding amacrine cell may provide a blue-off signal in a mammalian retina. Nat. Neurosci. *15*, 954–956.
11. Miyagishima, K.J., Grünert, U., and Li, W. (2014). Processing of S-cone signals in the inner plexiform layer of the mammalian retina. Vis. Neurosci. *31*, 153–163.
12. Dacey, D.M., Peterson, B.B., and Robinson, F.R. (2002). Identification of an S-cone opponent OFF pathway in the Macaque monkey retina: Morphology, physiology and possible circuitry. Investig. Ophthalmol. Vis. Sci. *43*, 2983.
13. Peng, Y.R., Shekhar, K., Yan, W., Herrmann, D., Sappington, A., Bryman, G.S., van Zyl, T., Do, M.T.H., Regev, A., and Sanes, J.R. (2019). Molecular Classification and Comparative Taxonomics of Foveal and Peripheral Cells in Primate Retina. Cell *176*, 1222–1237.e22.
14. MacNeil, M.A., and Masland, R.H. (1998). Extreme diversity among amacrine cells: implications for function. Neuron *20*, 971–982.
15. Roorda, A., and Williams, D.R. (1999). The arrangement of the three cone classes in the living human eye. Nature *397*, 520–522.
16. Liao, H.W., Ren, X., Peterson, B.B., Marshak, D.W., Yau, K.W., Gamlin, P.D., and Dacey, D.M. (2016). Melanopsin-expressing ganglion cells on macaque and human retinas form two morphologically distinct populations. J. Comp. Neurol. *524*, 2845–2872.
17. Patterson, S.S., Kuchenbecker, J.A., Anderson, J.R., Bordt, A.S., Marshak, D.W., Neitz, M., and Neitz, J. (2019). An S-cone circuit for edge detection in the primate retina. Sci. Rep. *9*, 11913.
18. Kolb, H., Goede, P., Roberts, S., McDermott, R., and Gouras, P. (1997). Uniqueness of the S-cone pedicle in the human retina and consequences for color processing. J. Comp. Neurol. *386*, 443–460.
19. Mariani, A.P. (1984). Bipolar cells in monkey retina selective for the cones likely to be blue-sensitive. Nature *308*, 184–186.
20. Euler, T., Haverkamp, S., Schubert, T., and Baden, T. (2014). Retinal bipolar cells: elementary building blocks of vision. Nat. Rev. Neurosci. *15*, 507–519.
21. Dacey, D.M., and Lee, B.B. (1994). The 'blue-on' opponent pathway in primate retina originates from a distinct bistratified ganglion cell type. Nature *367*, 731–735.
22. Calkins, D.J., Tsukamoto, Y., and Sterling, P. (1998). Microcircuitry and mosaic of a blue-yellow ganglion cell in the primate retina. J. Neurosci. *18*, 3373–3385.
23. Nasir-Ahmad, S., Lee, S.C.S., Martin, P.R., and Grünert, U. (2019). Melanopsin-expressing ganglion cells in human retina: Morphology, distribution, and synaptic connections. J. Comp. Neurol. *527*, 312–327.
24. Hannibal, J., Christiansen, A.T., Heegaard, S., Fahrenkrug, J., and Kiilgaard, J.F. (2017). Melanopsin expressing human retinal ganglion cells: Subtypes, distribution, and intraretinal connectivity. J. Comp. Neurol. *525*, 1934–1961.
25. Grünert, U., Jusuf, P.R., Lee, S.C.S., and Nguyen, D.T. (2011). Bipolar input to melanopsin containing ganglion cells in primate retina. Vis. Neurosci. *28*, 39–50.
26. London, M., and Häusser, M. (2005). Dendritic computation. Annu. Rev. Neurosci. *28*, 503–532.
27. Koontz, M.A. (1993). GABA-immunoreactive profiles provide synaptic input to the soma, axon hillock, and axon initial segment of ganglion cells in primate retina. Vision Res. *33*, 2629–2636.
28. Koontz, M.A., Hendrickson, A.E., and Ryan, M.K. (1989). GABA-immunoreactive synaptic plexus in the nerve fiber layer of primate retina. Vis. Neurosci. *2*, 19–25.
29. Werblin, F.S. (2011). The retinal hypercircuit: a repeating synaptic interactive motif underlying visual function. J. Physiol. *589*, 3691–3702.

30. Sher, A., and DeVries, S.H. (2012). A non-canonical pathway for mammalian blue-green color vision. Nat. Neurosci. *15*, 952–953.
31. Pérez De Sevilla Müller, L., Shelley, J., and Weiler, R. (2007). Displaced amacrine cells of the mouse retina. J. Comp. Neurol. *505*, 177–189.
32. Kolb, H., Linberg, K.A., and Fisher, S.K. (1992). Neurons of the human retina: a Golgi study. J. Comp. Neurol. *318*, 147–187.
33. Puller, C., and Haverkamp, S. (2011). Bipolar cell pathways for color vision in non-primate dichromats. Vis. Neurosci. *28*, 51–60.
34. Haverkamp, S., Wässle, H., Duebel, J., Kuner, T., Augustine, G.J., Feng, G., and Euler, T. (2005). The primordial, blue-cone color system of the mouse retina. J. Neurosci. *25*, 5438–5445.
35. Mollon, J.D. (1989). "Tho' she kneel'd in that place where they grew..." The uses and origins of primate colour vision. J. Exp. Biol. *146*, 21–38.
36. Lucas, R.J., Peirson, S.N., Berson, D.M., Brown, T.M., Cooper, H.M., Czeisler, C.A., Figueiro, M.G., Gamlin, P.D., Lockley, S.W., O'Hagan, J.B., et al. (2014). Measuring and using light in the melanopsin age. Trends Neurosci. *37*, 1–9.
37. Spitschan, M., Lucas, R.J., and Brown, T.M. (2017). Chromatic clocks: Color opponency in non-image-forming visual function. Neurosci. Biobehav. Rev. *78*, 24–33.
38. Mouland, J.W., Martial, F., Watson, A., Lucas, R.J., and Brown, T.M. (2019). Cones Support Alignment to an Inconsistent World by Suppressing Mouse Circadian Responses to the Blue Colors Associated with Twilight. Curr. Biol. *29*, 4260–4267.e4.
39. Woelders, T., Wams, E.J., Gordijn, M.C.M., Beersma, D.G.M., and Hut, R.A. (2018). Integration of color and intensity increases time signal stability for the human circadian system when sunlight is obscured by clouds. Sci. Rep. *8*, 15214.
40. Spitschan, M., Aguirre, G.K., Brainard, D.H., and Sweeney, A.M. (2016). Variation of outdoor illumination as a function of solar elevation and light pollution. Sci. Rep. *6*, 26756.
41. Pauers, M.J., Kuchenbecker, J.A., Neitz, M., and Neitz, J. (2012). Changes in the colour of light cue circadian activity. Anim. Behav. *83*, 1143–1151.
42. Packer, O.S., Verweij, J., Li, P.H., Schnapf, J.L., and Dacey, D.M. (2010). Blue-yellow opponency in primate S cone photoreceptors. J. Neurosci. *30*, 568–572.
43. Field, G.D., Sher, A., Gauthier, J.L., Greschner, M., Shlens, J., Litke, A.M., and Chichilnisky, E.J. (2007). Spatial properties and functional organization of small bistratified ganglion cells in primate retina. J. Neurosci. *27*, 13261–13272.
44. Della Santina, L., Kuo, S.P., Yoshimatsu, T., Okawa, H., Suzuki, S.C., Hoon, M., Tsuboyama, K., Rieke, F., and Wong, R.O.L. (2016). Glutamatergic Monopolar Interneurons Provide a Novel Pathway of Excitation in the Mouse Retina. Curr. Biol. *26*, 2070–2077.
45. Anderson, J.R., Mohammed, S., Grimm, B., Jones, B.W., Koshevoy, P., Tasdizen, T., Whitaker, R., and Marc, R.E. (2011). The Viking viewer for connectomics: scalable multi-user annotation and summarization of large volume data sets. J. Microsc. *241*, 13–28.
46. Cardona, A., Saalfeld, S., Schindelin, J., Arganda-Carreras, I., Preibisch, S., Longair, M., Tomancak, P., Hartenstein, V., and Douglas, R.J. (2012). TrakEM2 software for neural circuit reconstruction. PLoS ONE *7*, e38011.
47. Briggman, K.L., Helmstaedter, M., and Denk, W. (2011). Wiring specificity in the direction-selectivity circuit of the retina. Nature *471*, 183–188.
48. Dowling, J.E., and Boycott, B.B. (1966). Organization of the primate retina: electron microscopy. Proc. R. Soc. Lond. B Biol. Sci. *166*, 80–111.
49. Patterson, S.S., Bordt, A.S., Girresch, R.J., Linehan, C.M., Bauss, J., Yeo, E., et al. (2019). Wide-field amacrine cell input to ON parasol ganglion cells in macaque retina. J. Comp. Neurol. 1–11 https://doi.org/10.1002/cne.24840.
50. Tsukamoto, Y., and Omi, N. (2016). ON Bipolar Cells in Macaque Retina: Type-Specific Synaptic Connectivity with Special Reference to OFF Counterparts. Front. Neuroanat. *10*, 104.
51. Jusuf, P.R., Lee, S.C.S., Hannibal, J., and Grünert, U. (2007). Characterization and synaptic connectivity of melanopsin-containing ganglion cells in the primate retina. Eur. J. Neurosci. *26*, 2906–2921.
52. Dacey, D.M. (2004). Origins of perception: Retinal ganglion cell diversity and the creation of parallel visual pathways. In The Cognitive Neurosciences, M.S. Gazzaniga, ed. (MIT Press), pp. 281–301.
53. Dhande, O.S., Stafford, B.K., Franke, K., El-Danaf, R., Percival, K.A., Phan, A.H., Li, P., Hansen, B.J., Nguyen, P.L., Berens, P., et al. (2019). Molecular Fingerprinting of On-Off Direction-Selective Retinal Ganglion Cells Across Species and Relevance to Primate Visual Circuits. J. Neurosci. *39*, 78–95.
54. Tsukamoto, Y., and Omi, N. (2015). OFF bipolar cells in macaque retina: type-specific connectivity in the outer and inner synaptic layers. Front. Neuroanat. *9*, 122.
55. Puthussery, T., Gayet-Primo, J., Taylor, W.R., and Haverkamp, S. (2011). Immunohistochemical identification and synaptic inputs to the diffuse bipolar cell type DB1 in macaque retina. J. Comp. Neurol. *519*, 3640–3656.
56. Kim, H.L., Jeon, J.H., Koo, T.H., Lee, U.Y., Jeong, E., Chun, M.H., Moon, J.I., Massey, S.C., and Kim, I.B. (2012). Axonal synapses utilize multiple synaptic ribbons in the mammalian retina. PLoS ONE *7*, e52295.
57. Østergaard, J., Hannibal, J., and Fahrenkrug, J. (2007). Synaptic contact between melanopsin-containing retinal ganglion cells and rod bipolar cells. Invest. Ophthalmol. Vis. Sci. *48*, 3812–3820.

STAR★METHODS

KEY RESOURCES TABLE

REAGENT or RESOURCE	SOURCE	IDENTIFIER
Biological Samples		
Macaque retina	Regional Primate Research Center	N/A
Software and Algorithms		
Illustrator	Adobe	https://adobe.com/
MATLAB	Mathworks	RRID: SCR_001622
Nornir	Marc/Jones Lab, Utah	RRID: SCR_003584
SBFSEM-Tools	Neitz Lab, Washington	RRID: SCR_017350
Vikings	Marc/Jones Lab, Utah	RRID: SCR_005986

LEAD CONTACT AND MATERIALS AVAILABILITY

Further information and requests for resources should be directed to and will be fulfilled by the Lead Contact, Jay Neitz (jneitz@uw.edu). This study did not generate any new unique reagents.

EXPERIMENTAL MODEL AND SUBJECT DETAILS

Retinal tissue was obtained from a terminally anesthetized male macaque (*Macaca nemestrina*) monkey through the Tissue Distribution Program at the Washington National Primate Center. All procedures were approved by the Institutional Animal Care and Use Committee at the University of Washington.

METHOD DETAILS

Microscopy

The tissue was imaged using a Zeiss Sigma VP field emission scanning electron microscope equipped with a 3View system and sectioned in the horizontal plane. Tissue preparation and image collection were optimized in signal-to-noise ratio for visualizing small, low contrast features such as synaptic ribbons that have previously been a challenge for serial block-face scanning (Figures 2A and 2B). In each 90 nm section, an area approximately 200 μm on a side was imaged as a 5 X 5 montage at a resolution of 7.5 nm/pixel. The volume contained 1893 horizontal 90 nm sections from the ganglion cell layer through the cone pedicles. Image registration was performed using Nornir (http://nornir.github.io).

Tissue Preparation

A block of inferior parafoveal retinal tissue at ~1 mm eccentricity from the fovea center was processed as previously described [44]. A transmission electron microscopic image of a cross-section of the retina can be seen in Figure 1A of our previously published work [17]. Briefly, the eyecup was placed in 4% glutaraldehyde in 0.1M sodium cacodylate buffer pH 7.4 and while in this solution a 1 mm square of retina centered 1.5 mm inferior to the center of the fovea was cut out and then fixed overnight at 4°C. The tissue was next washed 5 × 5 min in 0.1M coacodylte buffer, then post fixed in osmium ferrocyanide for 1 h on ice. The tissue was next washed 5 × 5 min in double distilled (dd)H2O at room temperature (RT) and incubated in a 1% thiocarbohydrazide solution for 20 min at RT. The tissue was washed 5 × 5 min in ddH2O and placed in 2% osmium tetroxide for 30 min at RT. The tissue was next washed 5 × 5 min in ddH2O and en block stained in 1% uranyl acetate, (aqueous), overnight in the refrigerator. The next day the tissue was washed 5 × 5 min in ddH2O, then en bloc stained in Walton's lead aspartate for 30 min at 60°C. The tissue as next washed 5 × 5 min in ddH2O and dehydrated in ice cold 30%, 50%, 70%, and 95% ETOH, then allowed to come to RT. This was followed by 2 changes of 100% ETOH and two changes of propylene oxide. The tissue was then infiltrated in a 1:1 mixture of propylene oxide:Durcupan resin, for 2 h and then infiltrated overnight in fresh Durcupan. The next day the tissue was given a fresh change of Durcupan for two h and then placed in flat embedding molds and polymerized in a 60°C oven for two days. The block was then trimmed to approximately 0.5 mm^2. At this eccentricity (the edge of the foveal slope), the displacement of RGCs from cone pedicles was minimized while still remaining in a region where most midget RGCs receive single cone input.

Annotation

The serial EM volumes were annotated using the web-based, multiuser Viking software described previously (http://connectomes.utah.edu) [45]. Neuronal processes were traced through the sections by placing a circular disc at the structure's center of mass and

linking the disc to annotations on neighboring sections. Compared to contouring [46] and skeleton reconstruction [47], this connectomics approach provided an optimal balance of efficiency and resolution for circuit-level research questions [45]. There were two exceptions to the disc annotations. Cone pedicles were outlined using a closed curve polygon defined by three or more control points. The detailed morphological reconstruction in Figure 3G was obtained by manually tracing the outlines of each dendritic process.

Synapses were annotated with lines connected by 2-3 control points and linked to a parent neuron. Synapse identification used previously described parameters [48]. The boundaries of the inner plexiform layer were determined locally and marked throughout the volume with a total of 258 markers for the inner nuclear layer (INL) boundary and 453 markers for the IPL-ganglion cell layer (GCL) boundary.

Data Analysis and Visualization

Data analysis and 3D rendering were performed using SBFSEM-tools, an open-source MATLAB (Mathworks) program developed in the Neitz lab (https://github.com/neitzlab/sbfsem-tools) [17, 49]. Final figures were compiled in Adobe Illustrator.

The cone pedicle locations in Figure 1A were based on XYZ coordinates of the closed curve annotation control points, connected by Catmull-Rom splines. The detailed morphology reconstructions in Figure 3G were obtained by extracting the coordinates from a stack of manually annotated processes. These coordinates were used to build a volume from which isosurfaces were extracted with a marching cubes algorithm then rendered as a triangle mesh. All other analyses and visualizations were performed using the X, Y, Z coordinates and radius of each annotation. The 3D models are triangle meshes built by rendering segments of connected annotations as rotated cylinders centered at each annotations' XYZ coordinates and scaled by their radii.

INL-IPL and GCL-IPL boundary surfaces were fit to the X, Y and Z coordinates of each IPL boundary marker type using bicubic interpolation. IPL depth could then be calculated for each annotation individually. Given an annotation's X, Y coordinates, the surfaces supplied the depth of the IPL boundaries at that X,Y location. The annotation's Z coordinate relative to the Z coordinates of each boundary could be calculated to determine percent IPL depth.

Cell Type Identification

In addition to the S-ON bipolar cell verification described in the text and our previous work [17], we also verified the S-ON bipolar cells were distinct from the other two bipolar cell inputs stratifying in S5. The morphology of our DB6 reconstructions matched previous reports [25, 50]. A reliable parameter for distinguishing S-ON and DB6 bipolar cells is the smaller diameter of their axon terminal branches. Rod bipolar cell terminals were distinguished by input exclusively from rod photoreceptors in the outer retina and an absence of ribbon synapses onto RGCs in the inner retina.

To verify the identity of outer-stratifying (M1) ipRGCs, our strongest criteria was the dendritic stratification depth at the IPL-INL border [23, 24, 51]. Of all reported primate RGCs, M1 ipRGCs stratify closest to the inner nuclear layer (giant sparse monostratified [52]). The next closest RGC to the inner nuclear layer is the large sparse monostratified RGC, which stratifies around 30% IPL depth [52, 53]. The M1 ipRGCs in this study stratified between 0%–20%. Some primary dendrites of the M1 ipRGCs with somas in the ganglion cell layer traveled through S5 for tens of microns before descending to S1. However, all primary dendrites either reached S1 or ran off the edge of the volume. Displaced M1 ipRGCs are the only known RGC with a soma in the INL, providing further confirmation for the displaced M1 ipRGC (green) in Figure 1E, which stratified closest to the INL, had a large soma with significant synaptic input from a single amacrine cell type and a single axon with an ultrastructure and morphology matching the axons of RGCs in the ganglion cell layer. We also confirmed the presence of previously reported synaptic inputs. M1 ipRGCs receive some ON bipolar cell input in S1 from *en passant* synapses from DB6 bipolar cell axons, as well as other non-DB6 bipolar cell input presumed to be from DB1 bipolar cells [25]. We observed both M1 ipRGCs receiving infrequent bipolar cell input in S1 from neurons matching the morphology of DB1 bipolar cells [54, 55]. Several DB6 bipolar cell axons were reconstructed, however, *en passant* ribbon synapses in bipolar cell axons are smaller than ribbon synapses in bipolar cell terminals [56] and were difficult to reliably identify with our volume's resolution. No contacts were observed between ipRGC dendrites and S-ON bipolar cells or the S-cone OFF midget bipolar cells identified in our previous work [17]. In one case, appositions between a rod bipolar cell and an M1 ipRGC dendrite were observed [24, 57]. As previously reported, a single type of amacrine cell made large inhibitory synapses along the dendrites of M1 ipRGCs and the soma of the displaced M1 ipRGC. While none were traced back to a soma, their morphology was consistent with dopaminergic amacrine cells reported to provide extensive synaptic input to M1 ipRGC somas and dendrites [16].

QUANTIFICATION AND STATISTICAL ANALYSIS

No statistical tests were used in the manuscript.

DATA AND CODE AVAILABILITY

The 3D reconstructions from Viking Viewer annotations are visualized with SBFSEM-tools, an open-source MATLAB toolbox (https://github.com/neitzlab/sbfsem-tools). The Viking Viewer software for visualizing both the dataset and the annotations is freely available (http://connectomes.utah.edu). Raw data and additional analysis code will be provided upon request by the Lead Contact, Jay Neitz (jneitz@uw.edu).